University of Dundee

Predicting vortex merging and ensuing turbulence characteristics in shear layers from initial conditions

Anirban Guha[1],[2]† and Mona Rahmani[3]

[1]Institute of Coastal Research, Helmholtz-Zentrum Geesthacht,, Geesthacht 21502, Germany.

[2]School of Science and Engineering, University of Dundee, Dundee DD1 4HN, UK.

[3]Department of Mathematics, The University of British Columbia, 1984 Mathematics Road, Vancouver, British Columbia V6T 1Z2, Canada.

Unstable shear layers in environmental and industrial flows roll up into a series of vortices, which often form complex nonlinear merging patterns like pairs and triplets. These patterns crucially determine the subsequent turbulence, mixing and scalar transport. We show that the late-time, highly nonlinear merging patterns are predictable from the linearized initial state. The initial asymmetry between consecutive wavelengths of the vertical velocity field provides an effective measure of the strength and pattern of vortex merging. The predictions of this measure are substantiated using direct numerical simulations. We also show that this measure has significant implications in determining the route to turbulence and the ensuing turbulence characteristics.

1. Introduction

Vortex merging is an important mechanism in the evolution process of a series of adjacent co-rotating vortices (Lansky *et al.* 1997). This aesthetically pleasing pattern formation has appealed both artists and scientists, an evidence of the former is the famous painting – *The Starry Night* by the 19th century Dutch post-impressionist Vincent van Gogh. Vortex merging commonly occur in shear layers in the oceans (Flament *et al.* 2001), terrestrial (Buban & Ziegler 2016) and planetary atmospheres (Mac Low & Ingersoll 1986), impinging jets (Popiel & Trass 1991; Hwang *et al.* 2001), combustible jet flames (Demare & Baillot 2001), as well as in less regularly expected areas like the wake of mechanical heart valves (Bluestein *et al.* 2000). The primary vortices arise from the growth of Kelvin-Helmholtz (KH) instabilities on the interface of two fluids with different streamwise velocities. Through the process of merging, two (or more) neighbouring vortices are advected toward each other and merge into a larger vortex (Zaman & Hussain 1980). Vortex merging can significantly enhance the mixing induced by the evolution and turbulent breakdown of KH billows by providing more stirring of the fluids in the two fluid layers (Rahmani *et al.* 2014). This enhanced mixing has important implications for the estimations of vertical mixing of heat, nutrients and pollutants in the atmosphere, oceans and lakes (Ivey *et al.* 2008).

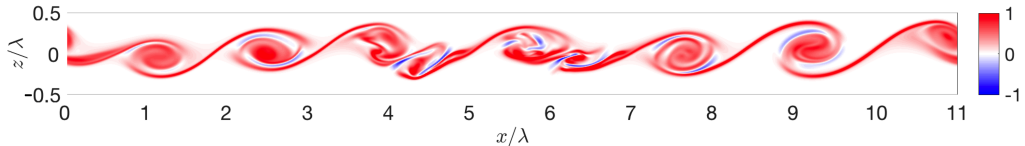† Email address for correspondence: anirbanguha.ubc@gmail.com

Figure 1: Irregular vortex merging patterns of eleven wavelengths, $\lambda = 2\pi/k$, (of the primary KH) in a density stratified shear layer initially perturbed with random noise (results from a fully 3D DNS). Two pairing events are currently undergoing at the time instant shown, while two pairing events have already taken place. Hence, although initially there were eleven primary KH billows, at present only nine vortices are left. Vorticity contours have been plotted. Negative vorticity primarily ensues from the baroclinic generation.

In this paper we show that the complex, *nonlinear* vortex merging patterns are predictable from the *linear initial conditions*. Such merging patterns are illustrated in figure 1, where a numerical simulation of a shear layer susceptible to KH instabilities has been initiated with a pure random noise. The asymmetrical structure of the KH billows leads to the merging of neighbouring vortices, albeit in a highly non-uniform way. Similar merging patterns have also been observed in laboratory experiments (Ho & Huang 1982), which indicate the growth of higher subharmonics. The numerical work of Baty & Keppens (2006), which investigated multiple wavelengths of the primary KH mode occurring in magnetized jets relevant to astrophysical flows, also reported complex merging patterns. Experiments by Unal & Rockwell (1988) and Williamson & Roshko (1988) showed the occurrence of vortex pairing as well as evidence of higher subharmonics in the near wake of a circular cylinder. Equivalent experimental observations were also reported by Rajagopalan & Antonia (2005), who further concluded that the near wake region behaves similar to a shear layer. The field observations of the oceanic horizontal shear layer past the island of Hawaii by Flament *et al.* (2001) revealed that the anticyclonic vortices formed on this shear layer proceeded to successively merge to form the first, second and third subharmonics of the original instability.

Experiments (Husain & Hussain 1995; Ho & Huang 1982), numerical simulations (Patnaik *et al.* 1976; Corcos & Sherman 1984; Dong *et al.* 2019) and theoretical models (Kelly 1967; Nikitopoulos & Liu 1987) on vortex pairing have revealed that depending on the phase difference (between the primary KH and the *first* subharmonic component), the outcome in the nonlinear stages can be radically different. An optimal phase difference leads to a "rolling interaction" of vortices, while "shredding interaction" occurs at a non-optimal value of phase difference. The former mode involves a dramatic engulfment of fluid by the merging vortices, whereas in the latter case, one weaker vortex is merely shredded by the strain field of the stronger vortex. The sensitivity of vortex pairing to phase difference has also been established in laboratory experiments with round jets (Arbey & Williams 1984; Broze & Hussain 1994; Paschereit *et al.* 1995). This phase difference can be used as a parameter for controlling the transitional behaviour, turbulence structure and mixing in shear layers (Hajj *et al.* 1993; Dong *et al.* 2019) and round jets (Cho *et al.* 1998), and even in noise control applications (Bridges & Hussain 1987; Schram *et al.* 2005).

While pairing is a nonlinear process and its dynamics has traditionally been described using weakly nonlinear theory (Kelly 1967; Monkewitz 1988), a recent study (Shaabani-Ardali *et al.* 2019) has demonstrated that self-sustained vortex pairing in a time-periodic jet is the manifestation of a subharmonic linear Floquet instability of the underlying

time-periodic vortex street. The present work also reveals that vortex pairing (and other merging patterns like triplets, quadruplets, etc.) in steady shear layers arise from a linear mechanism. However we take a very different approach in the present work – we provide a simple and mechanistic understanding of the role of subharmonics (not only the first, but any arbitrary subharmonic mode) on vortex merging in shear layers, which allows us to predict late-time merging patterns in multiple wavelengths of KH waves simply from the linear initial state.

2. Problem layout

We assume the classic vortex-sheet profile of KH instability (Batchelor 2000; Drazin & Reid 2004):

$$\bar{u}(z) = \begin{cases} U & z > 0 \\ -U & z < 0 \end{cases} \text{ and } \bar{\rho}(z) = \begin{cases} \rho_1 & z > 0 \\ \rho_2 & z < 0, \end{cases} \quad (2.1\text{a,b})$$

where $\bar{u}$ and $\bar{\rho}$ respectively denote the streamwise (x) background velocity and background density (with $\rho_2 \geqslant \rho_1$), and z points vertically upwards. The vortex sheet is perturbed by an infinitesimal sinusoidal disturbance of the form $\exp[\mathrm{i}(kx/\beta + ly - \Omega_\beta t)]$, where $k/\beta \in \mathbb{R}^+$ and $l \in \mathbb{R}^+$ are respectively the streamwise and spanwise wavenumbers, and $\Omega_\beta \in \mathbb{C}$ is the frequency.

Although the velocities at the interface are not defined, they can be calculated by taking the arithmetic mean of the velocities just above and below the interface. The perturbation vertical velocity at the interface is obtained by exploiting the linearized kinematic condition at the interface with $\bar{u} = 0$:

$$\frac{\partial \eta_\beta}{\partial t} + \bar{u}\frac{\partial \eta_\beta}{\partial x} = w_\beta = -\mathrm{i}\Omega_\beta \eta_\beta,$$

where η_β denotes the interface elevation. This shows that w_β has the same phase as η_β provided Ω_β is purely imaginary (unstable flow with zero phase speed).

The classic dispersion relation for KH instability under the Boussinesq approximation yields Drazin & Reid (2004):

$$\Omega_\beta \equiv \mathrm{i}\gamma_\beta = \pm\mathrm{i}\sqrt{\left(U\frac{k}{\beta}\right)^2 - Atg\tilde{k}}, \quad (2.2)$$

where γ_β is the growth rate, $\tilde{k} = \sqrt{(k/\beta)^2 + l^2}$, $At \equiv (\rho_2 - \rho_1)/(\rho_1 + \rho_2)$ is the Atwood number and g is gravitational acceleration. Equation (2.2) shows that for instability, Ω_β is purely imaginary, hence w_β and η_β have the same phase. This fact has a very important consequence in vortex merging, which will be elaborated in the following discussions.

For now we restrict ourselves to 2D flows (x–z) with polychromatic waves in the streamwise direction (note that now $l = 0$); k is the wavenumber of the primary mode and β is its ($\beta - 1$)th subharmonic; $\beta = 2, 3, \ldots$ Equation (2.2) shows that the growth rate γ_β is inversely proportional to β. Hence the primary mode has the fastest growth rate, and higher the subharmonic, the weaker is its growth rate. We first consider an interface perturbed by a dichromatic disturbance which has modes k and k/β. Hence the initial disturbance has the form

$$\eta(x, 0) = \hat{\eta}_1(0)\sin(kx) + \hat{\eta}_\beta(0)\sin(kx/\beta + \Phi_\beta),$$

where $\Phi_\beta \in [0, 2\pi)$ denotes the phase difference between the primary and the subharmonic

modes. This initial disturbance for a short time would evolve as

$$\eta(x,t) = \hat{\eta}_1(0)e^{\gamma_1 t}\sin(kx) + \hat{\eta}_\beta(0)e^{\gamma_\beta t}\sin(kx/\beta + \Phi_\beta),$$

provided t is small enough so that linearity of the system is respected.

2.1. Quantifying vortex merging from initial asymmetry

The physical mechanism behind vortex pairing is explained in figure 2. In figure 2(a-i), the first subharmonic mode (in red) tends to oppositely displace consecutive wavelengths of the primary mode (in black); the first wavelength (which gives rise to the first KH billow) moves upward while the second (which gives rise to the second KH billow) moves downward. The horizontal velocity shear advects the center of the billows toward each other, leading to pairing. If no asymmetry is introduced by the subharmonic mode, there wouldn't be any pairing; see figure 2(a-ii). The only difference between figure 2(a-i) and figure 2(a-ii) is the phase-shift, Φ_2. In a very similar manner, the second subharmonic induces pairing in figure 2(a-iii) but does not in figure 2(a-iv). The basis of the above argument is the fact that the interface elevation of any given mode and the corresponding vertical velocity are in phase.

Since asymmetry induced by the w velocity in two neighboring wavelengths of the primary mode leads to merging, we propose a quantitative measure that captures this effect. We consider two consecutive wavelengths of the primary mode and find the integral of the w velocity in each of them. The integrated w velocity due to the primary mode will always cancel out, but that due to the subharmonic mode can remain. We define a quantity $\mathcal{A}$ that measures the strength of the subharmonic mode induced asymmetry with respect to the w velocity amplitude of the primary mode. Mathematically we write it as follows:

$$\mathcal{A}_\beta^{(m,m+1)}(t) = \frac{\hat{w}_\beta(t)}{\hat{w}_1(t)}\left[\int_{2(m-1)\pi/k}^{2m\pi/k}\sin\left(\frac{k}{\beta}x + \Phi_\beta\right)dx - \int_{2m\pi/k}^{2(m+1)\pi/k}\sin\left(\frac{k}{\beta}x + \Phi_\beta\right)dx\right]$$

$$= -\frac{4\beta}{k}\frac{\gamma_\beta\hat{\eta}_\beta(0)}{\gamma_1\hat{\eta}_1(0)}e^{(\gamma_\beta-\gamma_1)t}\sin^2\left(\frac{\pi}{\beta}\right)\cos\left(\frac{2m\pi}{\beta} + \Phi_\beta\right). \qquad (2.3)$$

The prefix '$m, m+1$' of $\mathcal{A}_\beta$ signifies that we are comparing the m-th wavelength with the $(m+1)$-th wavelength of the primary mode, where the asymmetry is induced by the $(\beta-1)$-th subharmonic. The asymmetry is predicted after time t based on linear theory. Unless otherwise stated, we will evaluate the asymmetry at the initial time ($t = 0$). $\mathcal{A}_\beta^{(m,m+1)} > 0$ implies that two nearby vortices move towards each other and undergo merging, the higher the magnitude, the quicker is the merging. Likewise, $\mathcal{A}_\beta^{(m,m+1)} < 0$ implies that the two neighboring vortices move away from each other. We also note that, although the asymmetry seems directly proportional to β in Eq. (2.3), it is actually the opposite, which can be quickly verified from the terms γ_β/γ_1 and $\sin^2(\pi/\beta)$.

The phases leading to the maximum and minimum magnitudes of $\mathcal{A}_\beta^{(m,m+1)}$ are

$$\Phi_\beta^{max} = m\pi\left(1 - \frac{2}{\beta}\right) \text{ and } \pi\left[1 + m\left(1 - \frac{2}{\beta}\right)\right],$$

$$\Phi_\beta^{min} = \pi\left[\frac{1}{2} + m\left(1 - \frac{2}{\beta}\right)\right] \text{ and } \pi\left[\frac{3}{2} + m\left(1 - \frac{2}{\beta}\right)\right].$$

Figure figure 2(b) shows the variation of $\mathcal{A}_\beta^{(m,m+1)}$ with phase-shift. The asymmetry induced by the first and the second subharmonics have been separately computed.
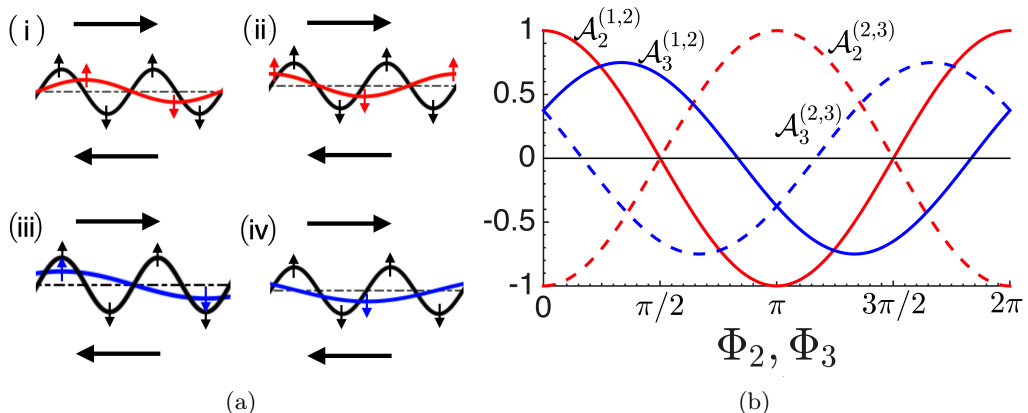
(a)   (b)

Figure 2: (a) Schematic showing the first two wavelengths of the primary mode of a KH instability, and its first and second subharmonic modes for different phase shifts. The horizontal (vertical) arrows represent horizontal (vertical) velocity. First subharmonic ($\beta = 2$) for (i) $\Phi_2 = 0$ (maximum asymmetry), and (ii) $\Phi_2 = \pi/2$ (minimum asymmetry). Second subharmonic ($\beta = 3$) for (iii) $\Phi_3 = \pi/3$ (maximum asymmetry), and (iv) $\Phi_3 = 5\pi/6$ (minimum asymmetry). (b) Variation of sample asymmetries with phase-shifts. Three consecutive wavelengths of the primary wave are considered. Red and blue color respectively indicate asymmetry induced by the first and the second subharmonics. While solid lines denote asymmetry between the first and the second primary waves, dashed lines denotes the same between the second and the third. The coefficient $4\beta\gamma_\beta\hat{\eta}_\beta(0)/(k\gamma_1\hat{\eta}_1(0))$ of $\mathcal{A}_\beta^{(m,m+1)}$ is assumed to be 1 in each case.

An important observation is that asymmetries between two different subharmonics can largely add-up or can largely cancel out. To elaborate this point further, let us assume that the interface is initially perturbed with the primary disturbance and its first and second subharmonics:

$$\eta(x,0) = \hat{\eta}_1(0)\sin(kx) + \hat{\eta}_2(0)\sin\left(\frac{k}{2}x + \Phi_2\right) + \hat{\eta}_3(0)\sin\left(\frac{k}{3}x + \Phi_3\right). \qquad (2.4)$$

Here 6 consecutive wavelengths of the primary wavelength need to be considered for observing the merging pattern (which would repeat after every six wavelengths). We do not consider any higher subharmonics ($\beta > 3$) since the growth-rate of these modes fall rapidly and are therefore of little consequence. We define the total asymmetry at $t = 0$ between two consecutive wavelengths (of the primary mode) as

$$\mathcal{A}_{total}^{(m,m+1)} = \mathcal{A}_2^{(m,m+1)} + \mathcal{A}_3^{(m,m+1)}. \qquad (2.5)$$

2.2. Predicting vortex merging from initial asymmetry

Depending on the phases Φ_2 and Φ_3, the asymmetries induced by these two subharmonics may largely add-up or may largely cancel out. For simplicity, we restrict to unstratified shear flows ($At = 0$). We span the entire Φ_2–Φ_3 space to see what combinations of these phase-shifts lead to high or low asymmetry. We also limit our analysis to initial amplitudes satisfying

$$(\hat{\eta}_2(0)/\hat{\eta}_1(0))^2 + (\hat{\eta}_3(0)/\hat{\eta}_1(0))^2 = 2.$$

In this respect three cases are considered:
- Case C1: $\hat{\eta}_2(0)/\hat{\eta}_1(0) = 1.41$ and $\hat{\eta}_3(0)/\hat{\eta}_1(0) = 0.11$,
- Case C2: $\hat{\eta}_2(0)/\hat{\eta}_1(0) = 1$ and $\hat{\eta}_3(0)/\hat{\eta}_1(0) = 1$,
- Case C3: $\hat{\eta}_2(0)/\hat{\eta}_1(0) = 0.11$ and $\hat{\eta}_3(0)/\hat{\eta}_1(0) = 1.41$.

Furthermore, since asymmetry depends on the wavelength-pair '$m, m+1$', we consider the maximum absolute asymmetry, i.e. $\max(|A_{total}|)$ among all '$m, m+1$' pairs, and plot it in figure 3. We observe that when the first subharmonic is very strong (figure 3(a)), $\max(|A_{total}|)$ is nearly independent of Φ_3; the asymmetry is nearly determined by Φ_2. However, increasing the relative strength of the second subharmonic increases the uniformity of $\max(|A_{total}|)$ in the Φ_2–Φ_3 space, as is clearly observed in figure 3(c). Hence a strong second subharmonic always yields moderate asymmetry independent of the phases.

While the above analysis revealed the importance of initial phase differences and amplitude ratios in deciding the 'global' picture of asymmetry (using $\max(|A_{total}|)$), the 'local' asymmetry $\mathcal{A}_{total}^{(m,m+1)}$ (obtained from (2.5)) is the key in providing quantitative estimates of the propensity towards vortex merging. To this end we keep

$$\hat{\eta}_2(0)/\hat{\eta}_1(0) = 1 \text{ and } \hat{\eta}_3(0)/\hat{\eta}_1(0) = 1,$$

and vary the initial phase differences:
- Case S1: $\Phi_2 = 0$ and $\Phi_3 = \pi$,
- Case S2: $\Phi_2 = \pi/2$ and $\Phi_3 = 0$,
- Case S3: $\Phi_2 = \pi/2$ and $\Phi_3 = \pi/2$.

The value of $\max(|A_{total}|)$ is 7 for S1, which is more than twice of the values corresponding to S2 ($\max(|A_{total}|) = 3$) and S3 ($\max(|A_{total}|) = 2.6$). Figure 4(a) corresponds to S1, and shows a moderately positive $\mathcal{A}_{total}^{(1,2)}$ and $\mathcal{A}_{total}^{(5,6)}$, a strongly positive $\mathcal{A}_{total}^{(3,4)}$, a strongly negative $\mathcal{A}_{total}^{(2,3)}$ and $\mathcal{A}_{total}^{(4,5)}$, and a weakly negative $\mathcal{A}_{total}^{(6,1)}$. This implies vortices 1–2 and 5–6 will slowly pair, while the pairing of 3–4 would be far rapid. Negative asymmetry implies that vortices will move away from each other, which we expect for both 2–3 and 4–5. While figure 4(a) has alternating positive and negative asymmetries (meaning the maximum extent of merging is *pairing*), figure 4(b) reveals a different picture – both 1–2 and 2–3 have positive asymmetries, while 3–4 has a negative one. This indicates the formation of *triplets*. Figure 4(c) indicates zero asymmetry for vortices 3–4 and 6–1, and are preceded by a negative asymmetry. This indicates that vortices 3 and 6 wouldn't undergo pairing. The veracity of all these predictions, made *solely* based on initial amplitude ratios and phase shifts, need to be substantiated using accurate numerical simulations. In fact, further late-time predictions from the initial asymmetry is also possible, and would be discussed in the following section.

3. Numerical simulations of shear instabilities and turbulence

Coherent structures appearing in transitional and turbulent shear flows can be accurately simulated using direct numerical simulations (DNS). To this end, we perform simulations using modest Reynolds number ($Re = 2000$, where $Re \equiv \Delta U h_0/\nu$; ν is the kinematic viscosity, ΔU and h_0 are respectively the shear velocity and length scales) DNS, that are more realizable in laboratory and/or industrial settings. The shear layer is initially assumed to be represented by $\bar{u} = \tanh(z)$; the velocity and the vertical coordinate z are respectively non-dimensionalized by $\Delta U/2$ and $h_0/2$. The governing 3D incompressible, non-dimensional Navier-Stokes equations are

$$\nabla \cdot \boldsymbol{u} = 0, \quad D\boldsymbol{u}/Dt = -\nabla p + Re^{-1}\nabla^2 \boldsymbol{u}, \tag{3.1a,b}$$
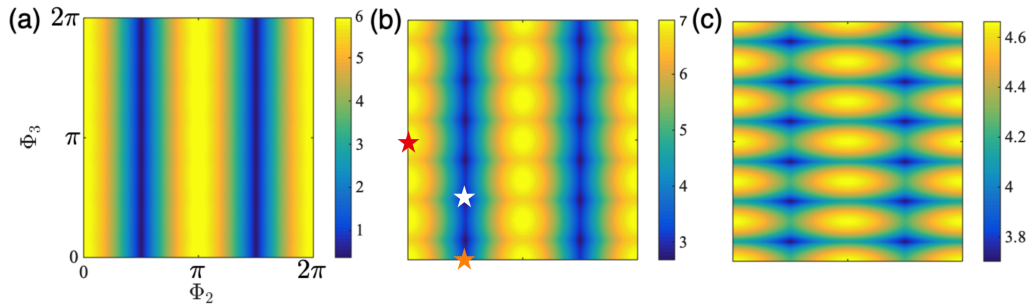
Figure 3: Maximum absolute asymmetry $\max(|A_{total}|)$ out of 6 consecutive wavelength pairs in an unstratified KH instability. The entire initial phase-shift space (Φ_2–Φ_3) is spanned. Results are shown for the following amplitude ratios: (a) Case C1, (b) Case C2, and (c) Case C3. Each sub-figure has its own colorbar. Red, orange and white stars respectively denote cases S1, S2 and S3.
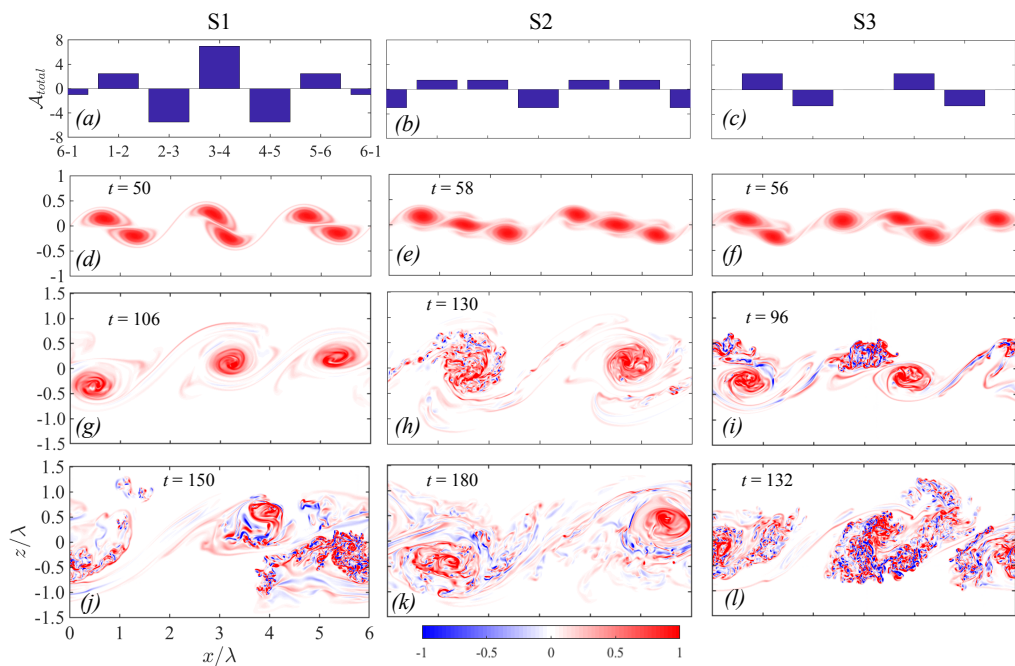

Figure 4: (a)-(c): Total asymmetry between consecutive wavelengths in an unstratified KH instability, inferred only from the linearized initial state. (d)-(f) Nonlinear evolution of KH instability using DNS during the first merging event. (g)-(i) Transition to turbulence in merged KH billows before the second merging event. (j)-(l) Turbulent phase of KH billows just before the last merging event. (a,d,g,j) Case S1, (b,e,h,k) Case S2, and (c,f,i,l) Case S3. The time t is non-dimensionalized by $h_0/\Delta U$.

where D/Dt denotes the material derivative, $\boldsymbol{u}$ denotes the dimensionless velocity vector and p denotes the dimensionless pressure. These equations are solved using a pseudo-spectral code described in detail by Winters *et al.* (2004) and Smyth *et al.* (2005). We keep the respective x, y and z dimensions as $(L_x, L_y, L_z) = (6\lambda_{KH}, 0.8\lambda_{KH}, 3\lambda_{KH})$,

where λ_{KH} denotes the wavelength of the most unstable KH mode. Each simulation is initially perturbed with the eigenfunctions of the primary KH and its first and second subharmonics with the right phase difference. The amplitudes of the eigenfunction perturbations are sufficiently small to ensure an initial linear growth of each mode. The eigenfunction perturbations are overlaid with random perturbations (of equal or smaller order of magnitude) to trigger 3D instabilities. The boundary conditions are periodic in both x and y directions and free slip at $z = 0$ and $z = L_z$. The number of mesh points used are: $(N_x, N_y, N_z) = (1152, 160, 576)$, which resolves the Kolmogorov length scale.

The DNS results for the cases S1–S3 during the first merging event are respectively shown in figures 4(d)-4(f). We find that the observed merging patterns are exactly as predicted by $\mathcal{A}_{total}^{(m,m+1)}$, shown in figures 4(a)-4(c), i.e. neighbouring vortices pair in the case S1, triplets form in the case S2 and alternative pairing/no-pairing occurs in the case S3. The phase relations between the primary mode and its subharmonics also have significant implications for the nonlinear evolution of the vortices in later stages and their turbulent breakdown, as shown in figures 4(g)-4(i) and 4(j)-4(l). In case S1, the merged vortices 1–2 and 5–6 undergo a second merging event, see figure 4(g). Finally, the merged vortices 3–4 coalesce with the merged vortices 1–2–5–6 to form a single vortex; this coalescence is underway in figure 4(j). The development of small-scale structures is delayed until the last merging event since most of the energy extracted from the background shear is spent on pairing (e.g. see Rahmani *et al.* (2014)).

For case S2, during the first merging event each three vortices form a triplet. The two merged triplets are fairly symmetric and their centers are far apart, hence they resist pairing for a relatively long time, see figure 4(h). Finally they undergo pairing after turbulent-like structures have grown in their cores, see figure 4(k). In case S3, the left-out vortices 3 and 6 eventually merge with vortices 4–5 and 1–2, respectively (figure 4(i)). This merging event is a "shredding interaction", and leads to the most vigorous disintegration of the core vortex, see figure 4(l).

Interestingly, $\mathcal{A}_{total}^{(m,m+1)}$ can also provide reasonable predictions of the second merging events. In other words, the large-scale 2D patterns observed in figures 4(g)-4(i), which respectively occur at $t = 150$, 180 and 132, are predictable from the $t = 0$ state (recall that $\mathcal{A}_{total}^{(m,m+1)}$ is always obtained from (2.5), which is the asymmetry evaluated at $t = 0$). Considering case S1, we already found from figure 4(a) that the first merging event leads to three vortex pairs: 1–2, 3–4 and 5–6 (figure 4(d)). If each primary KH billow has a circulation $\sim \Gamma$, then after the first merging event, each of the merged vortices 1–2, 3–4 and 5–6 will have a circulation $\sim 2\Gamma$. However $\mathcal{A}_{total}^{(2,3)} = \mathcal{A}_{total}^{(4,5)} = -5.5$, while $\mathcal{A}_{total}^{(6,1)} = -1$, implying that the merged vortices 5–6 and 1–2 are expected to be far closer to each other than they are individually with 3–4, hence the second merging would be between 1–2 and 5–6. The propensity towards this merging is observed in figure 4(g), and the merging is underway in figure 4(j), exactly as predicted.

Similar analyses can be done for the cases S2 and S3. For S2, the first merging event would lead to triplets 1–2–3 and 4–5–6, each with a circulation $\sim 3\Gamma$. Since $\mathcal{A}_{total}^{(6,1)} = \mathcal{A}_{total}^{(3,4)} = -3$, it implies that the two vortex triplets are far removed from each other, and hence resist second merging for a very long time, see figure 4(k). The case S3 is more interesting - the first merging produces vortex pairs 1–2 and 4–5, while vortices 3 and 6 are left out (figure 4(f)). Since $\mathcal{A}_{total}^{(2,3)} = \mathcal{A}_{total}^{(5,6)} = -2.6$ while $\mathcal{A}_{total}^{(3,4)} = \mathcal{A}_{total}^{(6,1)} = 0$, it implies that vortex 3 would merge with 4–5, while vortex 6 would merge with 1–2. Again, this prediction is exactly found to be true in figures 4(i) and 4(l).

The growth of turbulent-like coherent structures is a consequence of 3D motions
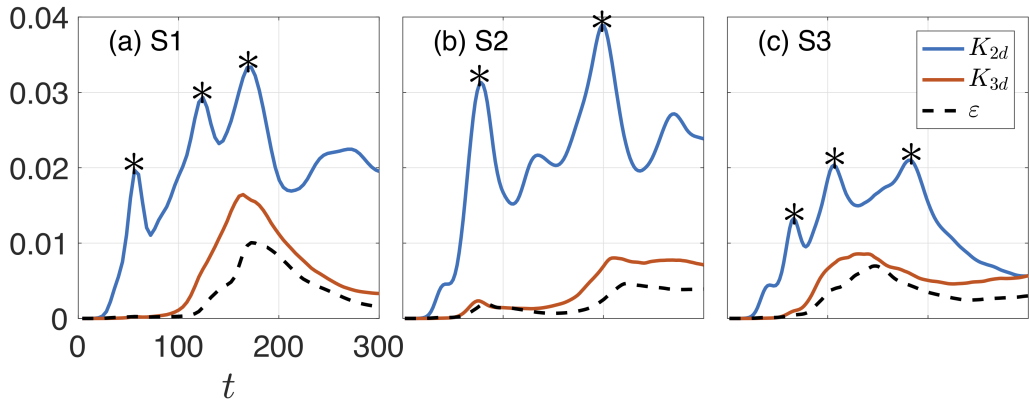
Figure 5: Time evolution of the dimensionless two- and three-dimensional kinetic energy, K_{2d} and K_{3d} and the rate of viscous dissipation of kinetic energy ε. The parameter ε has been multiplied by a factor of 20 for plotting. The peaks in K_{2d} corresponding to merging events are marked by stars.

extracting energy from the 2D flow. To quantify the strength of the 2D and 3D motions, and the intensity of turbulence, we utilize the definitions of the 2D kinetic energy: $K_{2d} = \langle \boldsymbol{u}_{2d} \cdot \boldsymbol{u}_{2d} \rangle_{xz}$, the 3D kinetic energy: $K_{3d} = \langle \boldsymbol{u}_{3d} \cdot \boldsymbol{u}_{3d} \rangle_{xyz}$, and the rate of viscous dissipation of the total kinetic energy: $\varepsilon = Re^{-1} \langle (\partial u_i / \partial x_j)^2 \rangle_{xyz}$, with $\langle \rangle$ denoting the averages in the specified directions (Caulfield & Peltier 2000). In these definitions the velocity field has been partitioned into three parts: $\overline{\boldsymbol{u}}(z) = \langle \boldsymbol{u} \rangle_{xy}$, $\boldsymbol{u}_{2d}(x,z) = \langle \boldsymbol{u} \rangle_y - \langle \boldsymbol{u} \rangle_{xy}$, and $\boldsymbol{u}_{3d}(x,y,z) = \boldsymbol{u} - \overline{\boldsymbol{u}} - \boldsymbol{u}_{2d}$. The competition between K_{2d} and K_{3d}, and the time evolution of ε, are shown in figure 5 for the cases S1-S3. Note that after the time shown (i.e. $t > 300$) all the motions start to decay. The intensity of the 2D and 3D motions and the viscous dissipation rate varies significantly between the different cases. The highest values in K_{2d} correspond to the case S2, where triplets are formed and the vertical extent of the merged vortices (i.e. inertial length scale) is the largest. The major local peaks in K_{2d} mark the merging events. For example, in cases S1 and S3, three merging events occur, while in the case S2, only two merging events occur. The global maxima in K_{3d} and ε occur close to the last merging event in the cases S1 and S2, and close to second merging in the case S3, where the second merging involves the agglomeration of the most asymmetric vortices. The peaks in K_{3d} and ε are the highest for S1 with the highest $\max(|A_{total}|)$. The values of the peaks of K_{3d} are almost the same for the cases S2 and S3 which have close values of $\max(|A_{total}|)$. We therefore conclude that the initial asymmetry of the primary KH wave with respect to its subharmonic modes, given by the global measure $\max(|A_{total}|)$, has significant implications for the intensity of the ensuing turbulence. For the highest $\max(|A_{total}|)$, vortex merging occurs either earlier (as in S1 compared to S2) or more energetically (as in S1 compared to S3). In the former case, the flow has more time to develop small-scale 3D turbulent motions before the decay starts (e.g. see Rahmani *et al.* (2014)) and in the latter case, the 3D motions can extract energy more efficiently from the 2D flow during the active turbulent phase. In both these situations, the higher $\max(|A_{total}|)$ has led to a higher intensity of turbulence.

4. Summary

In summary, we investigated the complex, multiple vortex merging patterns and ensuing turbulence characteristics in a shear layer. We have considered multiple wavelengths of the primary KH mode, and investigated the effect of higher subharmonics and not just the first subharmonic) on the primary KH for understanding the physics of vortex merging. While related previous studies that considered vortex array (Unal & Rockwell 1988; Rajagopalan & Antonia 2005; Baty & Keppens 2006; Shaabani-Ardali *et al.* 2019) have emphasized on the role of subharmonics in vortex merging, a simple physical understanding of the underlying mechanism seems to be missing. Based on the linear theory of KH instability arising in the classic vortex-sheet profile, we have provided a mechanistic understanding of the role of subharmonics in vortex merging. We have shown that the otherwise symmetric vertical velocity field of two neighboring wavelengths of the primary KH is rendered asymmetric by the presence of a subharmonic mode. This asymmetry, which is fully derived from the linear theory, is found to be the key in deciding the local merging patterns and their strengths. Based on the initial asymmetry of the vertical velocity profile, we have proposed an effective measure of vortex merging. Our analysis reveals that the highly nonlinear, local merging patterns in shear layers are predictable from the linearized initial state. Additionally, we show that subsequent merging patterns can also be predicted from the initial asymmetry. In fact, the highest amount of initial global asymmetry is found to yield the highest level of turbulence intensity. In summary, the main contribution of this paper is twofold – (i) to provide a simple, linear, mechanistic description of the role of subharmonics in vortex merging, and (ii) to predict nonlinear vortex merging patterns and ensuing turbulence characteristics from the linearized initial state.

In all our DNS studies reported in §3, the primary KH and the subharmonics are overlaid with random noise of comparable amplitude, and yet our model can still accurately predict the merging patterns from linear initial conditions. Only if the random noise, that can source from other concurrent phenomena in some realistic situations, is significantly stronger (and are nonlinear in nature) than the eigenfunction perturbations, we suspect that the predictive nature of the model, which relies on the linearity of the initial state, would break down.

Our findings imply that in many realistic situations, the route to turbulence, coherent structures and turbulent characteristics are strongly dependent on the initial disturbances. Therefore in future, it may be possible to engineer flows to achieve optimal turbulence and mixing.

Acknowledgement

REFERENCES

ARBEY, H. & WILLIAMS, J. E. FFOWCS 1984 Active cancellation of pure tones in an excited jet. *J. Fluid Mech.* **149**, 445–454.

BATCHELOR, G. K. 2000 *An Introduction to Fluid Dynamics*. Cambridge university press.

BATY, H. & KEPPENS, R. 2006 Kelvin-Helmholtz disruptions in extended magnetized jet flows. *Astron. Astrophys.* **447** (1), 9–22.

BLUESTEIN, D., RAMBOD, E. & GHARIB, M. 2000 Vortex shedding as a mechanism for free emboli formation in mechanical heart valves. *J. Biomed. Eng.* **122** (2), 125–134.

BRIDGES, J. E. & HUSSAIN, A. K. M. F. 1987 Roles of initial condition and vortex pairing in jet noise. *J. Sound Vib.* **117** (2), 289–311.

BROZE, G. & HUSSAIN, A. K. M. F. 1994 Nonlinear dynamics of forced transitional jets: periodic and chaotic attractors. *J. Fluid Mech.* **263**, 93–132.

BUBAN, M. S. & ZIEGLER, C. L. 2016 The formation of small-scale atmospheric vortices via horizontal shearing instability. *J. Atmos. Sci.* **73** (5), 2061–2084.

CAULFIELD, C. P. & PELTIER, W. R. 2000 The anatomy of the mixing transition in homogeneous and stratified free shear layers. *J. Fluid Mech.* **413**, 1–47.

CHO, S. K., YOO, J. Y. & CHOI, H 1998 Vortex pairing in an axisymmetric jet using two-frequency acoustic forcing at low to moderate strouhal numbers. *Exp. Fluids* **25** (4), 305–315.

CORCOS, G. M. & SHERMAN, F. S. 1984 The mixing layer: deterministic models of a turbulent flow. part 1. introduction and the two-dimensional flow. *J. Fluid Mech.* **139**, 29–65.

DEMARE, D. & BAILLOT, F. 2001 The role of secondary instabilities in the stabilization of a nonpremixed lifted jet flame. *Phys. Fluids* **13** (9), 2662–2670.

DONG, W., TEDFORD, E. W., RAHMANI, M. & LAWRENCE, G. A. 2019 Sensitivity of vortex pairing and mixing to initial perturbations in stratified shear flows. *Phys. Rev. Fluids* **4**, 063902.

DRAZIN, P. G. & REID, W. H. 2004 *Hydrodynamic stability*. Cambridge university press.

FLAMENT, P, LUMPKIN, R, TOURNADRE, J & ARMI, L 2001 Vortex pairing in an unstable anticyclonic shear flow: discrete subharmonics of one pendulum day. *J. Fluid Mech.* **440**, 401–409.

HAJJ, M. R., MIKSAD, R. W. & POWERS, E. J. 1993 Fundamental–subharmonic interaction: effect of phase relation. *J. Fluid Mech.* **256**, 403–426.

HO, C-M & HUANG, L-S 1982 Subharmonics and vortex merging in mixing layers. *J. Fluid Mech.* **119**, 443–473.

HUSAIN, H. S. & HUSSAIN, A. K. M. F. 1995 Experiments on subharmonic resonance in a shear layer. *J. Fluid Mech.* **304**, 343–372.

HWANG, S. D., LEE, C. H. & CHO, H. H. 2001 Heat transfer and flow structures in axisymmetric impinging jet controlled by vortex pairing. *Int. J. Heat Fluid Fl.* **22** (3), 293–300.

IVEY, G. N., WINTERS, K. B. & KOSEFF, J. R. 2008 Density stratification, turbulence, but how much mixing? *Annu. Rev. Fluid Mech.* **40**.

KELLY, RE 1967 On the stability of an inviscid shear layer which is periodic in space and time. *J. Fluid Mech.* **27** (4), 657–689.

LANSKY, I. M., O'NEIL, T. M. & SCHECTER, D. A. 1997 A theory of vortex merger. *Phys. Rev. Lett.* **79** (8), 1479.

MAC LOW, M-M & INGERSOLL, A. P. 1986 Merging of vortices in the atmosphere of Jupiter: An analysis of Voyager images. *Icarus* **65** (2-3), 353–369.

MONKEWITZ, P. A. 1988 Subharmonic resonance, pairing and shredding in the mixing layer. *J. Fluid Mech.* **188**, 223–252.

NIKITOPOULOS, D. E. & LIU, J. T. C. 1987 Nonlinear binary-mode interactions in a developing mixing layer. *J. Fluid Mech.* **179**, 345–370.

PASCHEREIT, C. O., WYGNANSKI, I & FIEDLER, H. E. 1995 Experimental investigation of subharmonic resonance in an axisymmetric jet. *J. Fluid Mech.* **283**, 365–407.

PATNAIK, P. C., SHERMAN, F. S. & CORCOS, G. M. 1976 A numerical simulation of Kelvin-Helmholtz waves of finite amplitude. *J. Fluid Mech.* **73** (2), 215–240.

POPIEL, C. O. & TRASS, O. 1991 Visualization of a free and impinging round jet. *Exp. Therm. Fluid Sci.* **4** (3), 253–264.

RAHMANI, M, LAWRENCE, G. A. & SEYMOUR, B. R. 2014 The effect of Reynolds number on mixing in Kelvin–Helmholtz billows. *J. Fluid Mech.* **759**, 612–641.

RAJAGOPALAN, S. & ANTONIA, R. A. 2005 Flow around a circular cylinderstructure of the near wake shear layer. *Exp. Fluids* **38** (4), 393–402.

SCHRAM, C, TAUBITZ, S, ANTHOINE, J & HIRSCHBERG, A 2005 Theoretical/empirical prediction and measurement of the sound produced by vortex pairing in a low Mach number jet. *J. Sound Vib.* **281** (1-2), 171–187.

SHAABANI-ARDALI, L., SIPP, D. & LESSHAFFT, L. 2019 Vortex pairing in jets as a global Floquet instability: modal and transient dynamics. *J. Fluid Mech.* **862**, 951–989.

SMYTH, W. D., NASH, J. D. & MOUM, J. N. 2005 Differential diffusion in breaking Kelvin-Helmholtz billows. *J. Phy. Oceanogr.* **35**, 1004–1022.

UNAL, M. F. & ROCKWELL, D. 1988 On vortex formation from a cylinder. part 2. control by splitter-plate interference. *J. Fluid Mech.* **190**, 513–529.

WILLIAMSON, C. H. K. & ROSHKO, A. 1988 Vortex formation in the wake of an oscillating cylinder. *J. Fluids Struct.* **2** (4), 355–381.

WINTERS, K. B., MACKINNON, J. A. & MILLS, B. 2004 A spectral model for process studies of rotating density-stratified flows. *J. Atmos. Ocean. Technol.* **21**, 69–94.

ZAMAN, K. B. M. Q. & HUSSAIN, A. K. M. F. 1980 Vortex pairing in a circular jet under controlled excitation. Part 1. General jet response. *J. Fluid Mech.* **101** (3), 449–491.